Thermal characterization of polyethylene glycol 600 in liquid, solid phases and through the phase transition

Justine Noel, Yves Jannot, Christel Métivier, Nicolò R Sgreva

Thermal characterization of polyethylene glycol 600 in liquid and solid phase and across the phase transition

Justine Noel[a], Yves Jannot[a], Christel Métivier[a,*], Nicolò R. Sgreva[a]

[a] *Université de Lorraine, LEMTA, CNRS, 54000 Nancy, France.*

Abstract

The polyethylene glycol (PEG) is characterized by experimental means in both solid and liquid phase. Main thermal properties inherent to the phase transition are also provided. More specifically, we focus on PEG 600, whose average molar mass is 600 g mol^{-1} and melting temperature transition is about 283-293 K. The phase change does not occur at a given temperature but rather over a range of temperature, highlighting the complexity of the material. Several methodologies have been developed and calibrated in order to obtain, in both phases, the density and the thermal conductivity. A temperature dependence fit is proposed for the density in liquid phase. The relative density variation from the liquid to solid phase is significant as it can reach about 35 %, meaning a quite large volume shrinkage. Differential Scanning Calorimetry (DSC) has been used for measuring the heat capacity of solid and liquid phase and the effective heat capacity at the transition states. The latent heat of fusion and solidification converge to a value of around 130 kJ kg^{-1}. Undercooling effects are mitigated by performing DSC with slow temperature variation rates. Lastly, we have also observed several exothermic peaks during the solidification process that are related to structural reorganizations of the material.

1. Introduction

Polyethylene glycol (PEG) is a polyether present in our daily life and its employment covers a wide range of industries, such as cosmetics, pharmaceuticals, food manufacturing, inks. As an example, it is used as a thickener

*christel.metivier@univ-lorraine.fr

agent in cosmetic products (liquid soaps, moisturizers, shampoos, etc.) and paramedical products (hydro-alcoholic gels, intimate lubricants [1], etc.). It is also used as a solvent in printer inks or to manufacture paint balls, as a food additive and in certain polyester resins. Because it is a bio-compatible product [2], it is also widely used in medical treatments and vaccines [3], as recently for Covid-19 vaccine. In addition, the polyethylene glycol presents remarkable properties: from a chemical viewpoint it is stable, non corrosive and non toxic. Another significant advantage lies in the large variety of temperatures at which the solid/liquid transition occurs. Depending on PEG's molecular weight, phase transition occurs for instance around 283-293 K for PEG 600, 321-323 K for PEG 1000 [4] and around 324 K for PEG 1500 [5]. For these reasons, numerous studies have been devoted to propose Composite Phase Change Materials (CPCMs) based on polyethylene glycol [6, 7, 8, 9, 10, 11, 12]. Phase change materials (PCMs) are widely studied in the field of energy storage/release since a large amount of energy can be transferred during the phase change via latent heat. Energy is stored during endothermic transformations (e.g. solid to liquid) while it is released during exothermic transformations. The large latent heat of PEG makes it a very interesting and attractive PCM. Furthermore, it matches perfectly the criteria related to the choice of PCMs, such as being low-cost, non-toxic, non-flammable, non-corrosive and biodegradable (bio-compatible), i.e. eco-friendly. The uses of PEG in Composite PCMs can concern thermal regulation in buildings [13] or pavements [8] as well as in photovoltaic panels [4, 12].

Despite the wide use of PEG, only few papers were devoted to characterize the thermal properties of polyethylene glycol alone. Recently, Kou et al. [14] have measured heat capacities of PEG for molar mass varying from 2000 to 20 000 g mol^{-1}. For smaller molar mass, as it is the case of PEG 600 (average molar mass of 600 g mol^{-1}), available data corresponds mainly to properties for the liquid phase only. For instance, density measurements are provided by several authors [15, 16, 17, 18], but they are given only for the liquid phase and only for few temperature values, not sufficient to obtain the thermal expansion coefficient. Some properties of PEG 600 are also given by Lane [19]. This paper focuses on properties of PCMs; for PEG 600, the author indicates the latent heat of melting and only one value for the melting temperature. Lane [19] also provides the thermal conductivity and the density in liquid phase for a couple of temperature values. Only a few other studies present the thermal conductivity of liquid phase, e.g. [17, 19].

Thus, properties of PEG remain partially and scatteredly described in the literature. Moreover, this small number of measured properties is obtained only for the liquid phase. To our knowledge, the latent heat of solidification, the freezing point, the thermal conductivity, the density and the heat capacity for the solid phase are not available in the literature.

From a structural viewpoint, PEG's properties - in particular at the solid/liquid transition - depend not only on the molecular weight but also on the protocols involved in measuring them. Several types of aggregate structures, such as helical or spherical conformations have been observed within the freezing process [20, 21]. Understanding the correlation between structural modifications and imposed experimental conditions is crucial since the structural organization can have a significant impact on the macroscopic properties. Indeed, in the case of semi-crystalline polymers as it is for PEG, Bogdanov et al. [22] highlighted the influence of the cooling rate on the exothermic crystallization peak by means of isothermal Differential Scanning Calorimetry (DSC). Furthermore, a correlation between the heat flux measured by DSC and the degree of crystallinity of PEG is proposed by Pielichowski & Flejtuch [23].

As a first step in the understanding of the relationships between PEG's behaviour and conditions of use, we clarify and provide new macroscopic properties for PEG 600. The aim of our study is to characterize this polyether in both the solid and liquid phase. In the liquid phase, we provide original values of macroscopic properties and how they vary with temperature. In the solid phase, we aim to fill the data gap in the literature. We carefully detail the methodologies and protocols used to obtain the main thermal properties in each phase (density, effective heat capacity and thermal conductivity) and the latent heat of melting and solidification. In section 2, the different measurement techniques and protocols used are detailed. Results are provided in section 3 where they are also compared with the available literature. The paper ends with conclusions and perspectives.

2. Methods and experimental devices

2.1. Material

Polyethylene glycol (PEG) is a linear polyether made from ethylene glycol monomers characterized by a molar mass generally smaller than 20 000 $\mathrm{g\,mol^{-1}}$. In this study, we aim to characterize the polyethylene glycol with molar mass of around 600 $\mathrm{g\,mol^{-1}}$, named PEG 600 (see Table 1). Several

Table 1: Sample table

Chemical Name	Source	Initial Mole Fraction Purity	Purification Method	Final Mole Fraction Purity	Analysis Method
Polyethylene Glycol 600	Merck CAS 25322-68-3	570-630 g mol^{-1}	none	-	-

batches supplied by Merck (CAS 25322-68-3) have been used to verify reproducibility of results. The temperature of the solid-liquid phase change is indicated by the supplier within the range of 290.15-293.15 K.

2.2. Density

2.2.1. Liquid phase

The density (ρ) of PEG 600 in liquid phase is measured by using a densimeter DMA 5000M, Anton Paar. The densimeter provides a 10^{-6} g cm^{-3} accuracy in the temperature range of 273.15-333.15 K, while for larger temperatures (up to a maximum of 373.15 K) the accuracy decreases to 10^{-4} g cm^{-3}. The precision on the temperature is 0.01 K. Calibration and validation of the device are given in the supplementary material. Density measurements are carried out at constant pressure P (atmospheric pressure) and at different temperature values within the range of 294.15-373.15 K where PEG 600 is liquid. Isothermal conditions are obtained by imposing temperature steps with a 1 K increment in the range 294.15-323.15 K, followed by a 5 K increment up to the temperature of 373.15 K. In the liquid phase, the time to achieve the thermal stability is about 5 minutes per temperature step.

To ensure reproducible results, density is measured on three different samples (volume of $\sim$1 mL) from two different batches. At a given temperature, the maximal variation between measurements is found to be 10^{-4} g cm^{-3} and the final value of density is taken as the mean of these measurements. From the temperature dependence of the density, we evaluate the thermal expansion coefficient β as follows

$$\beta = -\frac{1}{\rho_{ref}} \left(\frac{\partial \rho}{\partial T} \right)_P , \tag{1}$$

with $\rho_{ref} = \rho(T_{ref})$ being a reference density defined at the temperature T_{ref}. The thermal expansion coefficient indicates the first-order density variations

Table 2: Pressure measurements performed for the pycnometer calibration - Steps (1) and (2). P_i is the initial pressure and P_f the final pressure [a].

Step (1)			Step (2)		
P_i (bar)	P_f (bar)	P_f/P_i	P_i (bar)	P_f (bar)	P_f/P_i
3.654	1.685	46.1 %	3.655	2.002	54.7 %
3.660	1.696	46.3 %	3.650	2.002	54.8 %
3.665	1.706	46.5 %	3.603	1.976	54.8 %

[a] Standard uncertainties u are u(P_i) = 0.002 bar, u(P_f) = 0.002 bar, and the combined expanded uncertainty Uc is Uc(P_f/P_i) = 0.2% with 0.95 level of confidence (k≈2).

with temperature (Boussinesq approximation) at constant pressure [24] and, for a given mass of a material, it also corresponds to the volume variation with temperature.

2.2.2. Solid phase

Density measurements in the solid phase is achieved using a lab-made pycnometer. Validation of the device is provided in the supplementary material. The device is placed in a thermostatic enclosure Binder^{TM} KBF 115 in order to control the temperature. The pycnometer consists in two different cavities of volume V and V' separated by a valve as represented in Fig. 1. The measurement procedure is to initially obtain the vacuum in both cavities, i.e. $P' = P = 0$, then close the valve and impose a pressure P_i to the lower cavity. The valve is then opened involving pressure variations until an equilibrium is reached within the two cavities, leading to a final pressure P_f. The pressure is measured using a Mano 2000 Leo 3 Keller with an accuracy of 1 mbar.

We first start by a calibration of the device, i.e. we determine the volumes V and V' of each cavity by repeating several times the above mentioned procedure through Steps (1) and (2), as indicated in Fig. 1 b. Volumes V and V' are determined via the following equation

$$P_i V = P_f \times (V + V' - V_{ref}), \tag{2}$$

where V_{ref} corresponds to the volume of a cylinder of height 0.02 m and radius 0.04 m. The procedure is repeated three times. Table 2 summarizes these measurements and shows the good stability in terms of pressure values (variation within 0.4 %).

Finally, Step (3) is performed with a given mass of PEG (Fig. 1 b). The temperature set in the binder is 273.75 K in order to have a fully solid

(a)

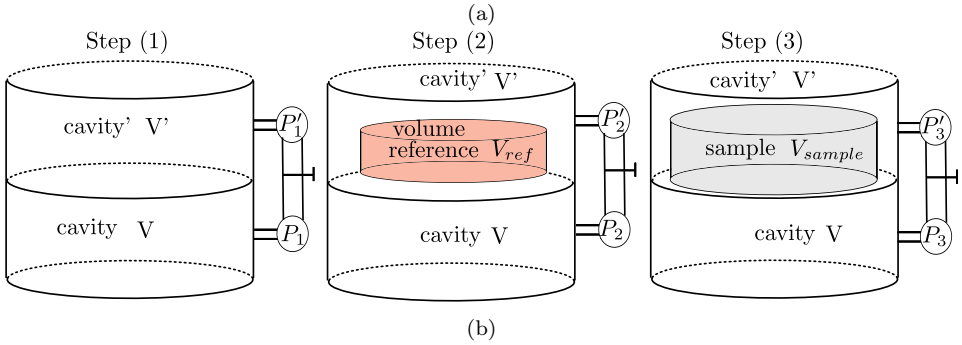

(b)

Figure 1: (a) Photo of the pycnometer. (b) Sketch of the set-up for calibration - Step (1) and Step (2) - and for measuring the density of solid PEG 600 - Step (3) -.

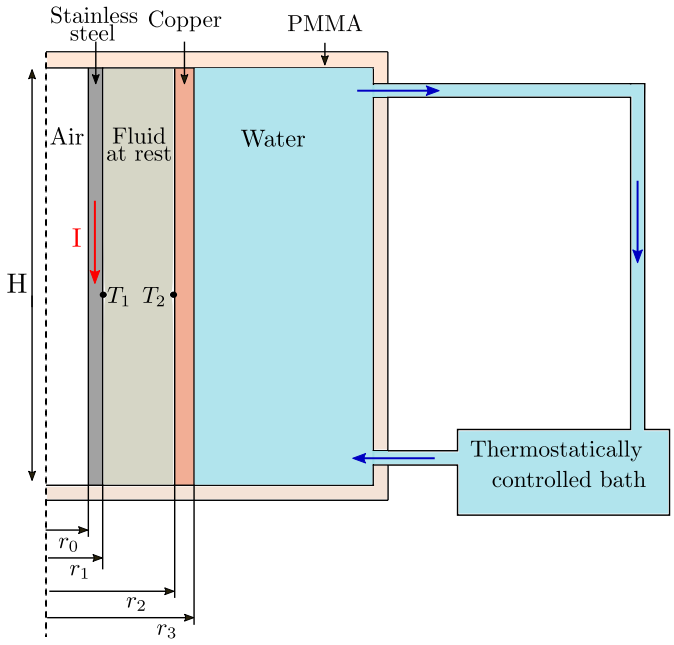

Figure 2: Sketch of the hot tube device used for thermal conductivity measurements. $r_0 = 2.54$ mm, $r_1 = 2.75$ mm, $r_2 = 6.00$ mm

sample. The volume of solid PEG is obtained using eq. (2) in which V_{ref} is replaced by the unknown sample volume. The density of PEG in solid phase is deduced from this measurement.

2.3. Thermal conductivity

2.3.1. Liquid phase

The thermal conductivity of the liquid phase is measured via the stationary hot tube method [25, 26]. A sketch of the device developed in our laboratory is shown in Fig. 2. A validation of the device with distilled water is provided in the supplementary material. The sample is introduced in liquid phase into the gap between two coaxial cylinders made of copper (the outer one) and stainless steel (the inner one). We ensure that the sample fills completely the space between the two cylinders, i.e. the space between r_1 and r_2 in Fig. 2. An electric current I is applied to the inner cylinder, producing heat flux by Joule effect. The outer part of the copper cylinder is maintained at a given temperature via a temperature controlled water flow. The temperatures T_1 and T_2 are measured using two type K thermocouples locked on the wall of the cylinders, i.e. at the boundaries of the liquid layer

(as indicated in Fig. 2). Moreover, in order to avoid any up-down wall effects, thermocouples are located at the mid-height of the device. The temperature difference is measured thanks to the voltage difference U between these two thermocouples:

$$\Delta T = T_1 - T_2 = U/k,$$

where k is a constant equal to $k = (39.2 + 0.064 \times T_2 - 0.005 \times T_2^2) \times 10^{-6}$ $\mathrm{V\,K^{-1}}$. Thermocouples are connected to a cold junction block. Tension and electrical current are measured with a Keysight U3401A and an ISO-TECH IDM91E multimeter, respectively.

For a purely conductive regime in the liquid layer (fluid at rest), the thermal conductivity can be deduced as follows [25]:

$$\lambda = \frac{\rho_{el} I^2 \ln(r_2/r_1)}{2\pi^2 (r_1^2 - r_0^2)\Delta T} \tag{3}$$

with $\rho_{el} = 7.3 \times 10^{-7}(1 + 1.36 \times 10^{-2}(T - T_{ref}))$ Ω m being the electrical resistivity of the stainless steel and T_{ref} a temperature reference equal to 293.15 K.

The dimensions of the device are determined under the condition that no convection occurs for a wide range of fluids. According to [27], we ensure that the following condition is satisfied:

$$\frac{Ra}{H^+} < 400 \tag{4}$$

where $H^+ = H/\delta$, H is the height of cylinders, $\delta = r_2 - r_1$ is the thickness of the liquid layer and Ra corresponds to the Rayleigh number given by

$$Ra = \frac{\rho g \beta \Delta T \delta^3}{\mu a}, \tag{5}$$

with μ being the dynamic viscosity and a the thermal diffusivity of the fluid.

This condition is verified a posteriori and in the case of our measurements with PEG we estimate $Ra/H^+ \approx 15 - 20 \ll 400$.

Device validation performed with water leads to a maximal difference in thermal conductivity of 2 % with values provided by Brown & Marco [28] (i.e. a variation of 0.01 $\mathrm{W\,m^{-1}\,K^{-1}}$). Since the device is filled by the PCM in liquid phase, the volume of the sample varies with the temperature with a

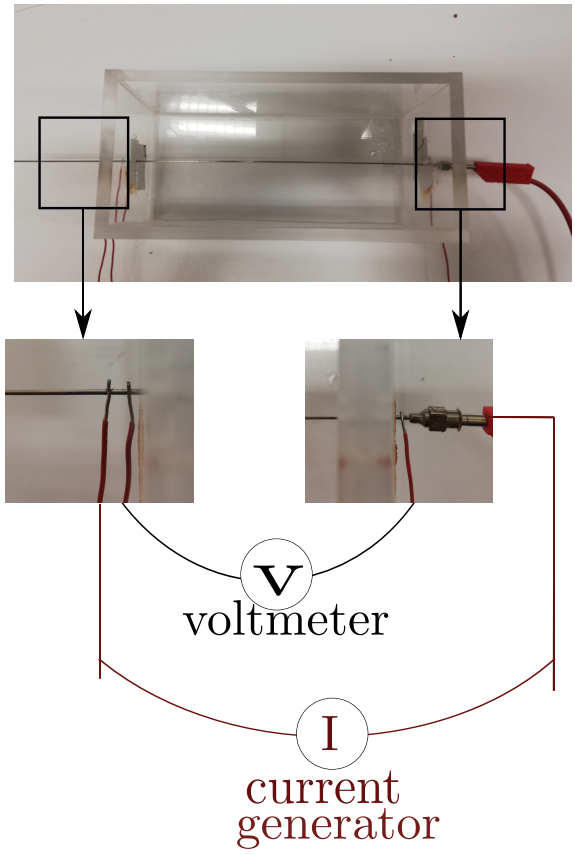

Figure 3: Photo of the heated needle device

maximal variation occurring during the phase transition. As it is with most materials, PEG decreases in volume from liquid to solid phase. This can lead to imperfect contacts at walls during the solidification, as detailed in Appendix A. In this case, i.e. when thermal contact resistances are present at walls, the device becomes unsuitable for measuring thermal conductivity of materials in solid phase. For this reason, we propose another technique to carry out measurements in the solid phase. This technique is detailed in the following paragraph.

2.3.2. Hot needle method

We developed a specific device in order to measure the thermal conductivity of materials in solid or liquid phase. The device consists in a $200 \times 120 \times 120$ mm^3 cavity made of PMMA that is filled with the sample.

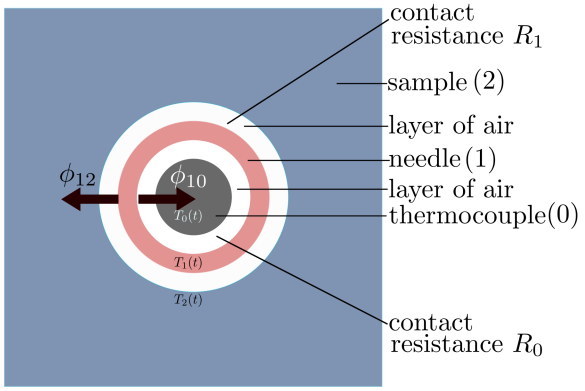

Figure 4: Schematic cross section of the hollow needle probe. The subscripts "0", "1" and "2" refer to the thermocouple, the needle and the sample, respectively.

A stainless steel hollow needle of length 300 mm is placed at the center of the device (Fig. 3). Needle's inner and outer radii are $r_i = 0.80$ mm and $r_e = 1.25$ mm, respectively. The needle is heated by Joule effect and the corresponding heat flow rate per unit of length L is $\phi = (UI)/L$, with U the electrical tension and I the electric intensity. Temperature is measured at the central point inside the needle with a K-type sheath thermocouple of radius $r_t = 0.5$ mm. Electrical tension and current are measured with a Tektronix DMM and an ISO-TECH IDM91E multimeter, respectively. Temperatures are recorded using a TC-08 Picolog device with a frequency of 10 Hz.

According to Fig. 4, in the following description we use the subscripts "0", "1" and "2" to refer to the thermocouple, the needle and the sample, respectively.

The device is placed in a Binder^{TM} KBF 115 thermostatic chamber in order to maintain the system at a controlled temperature. The thermostatic chamber also guarantee a constant initial temperature $T(t = 0)$ in the whole system, i.e. $T_0(0) = T_1(0) = T_2(0)$, being the initial temperatures of the thermocouple, the needle and the sample, respectively. We assume uniform temperature field in the needle, $T_1(t)$, and in the thermocouple, $T_0(t)$, since they are very thin. Moreover, since contacts at interface 1-2, i.e. needle-sample, and at the interface 1-0, i.e. needle-thermocouple, are not perfect, also the thermal contact resistances R_1 and R_0 (see Fig. 4) have to be taken into account. Finally, due to the long length of the cavity, we consider an unidirectional dependence of parameters at the center of the cavity.

As the needle is heated, the total heat flow rate ϕ due to Joule effect can

be split in two components, i.e. $\phi = \phi_{10} + \phi_{12}$ where ϕ_{12} is the heat transferred to the material and ϕ_{10} the heat transferred to the thermocouple. Heating the needle also induces transient variations in temperature within the whole system. Thermal properties of PEG can be obtained by considering the heat equation (conductive regime) in two domains assorted with boundary conditions. For this purpose, we use the quadrupole formalism proposed by Maillet *et al.* [29].

The first domain is bounded by the outer surface of the needle ($r_1 = r_e (\approx r_i)$) and a surface of the material sample ($r_2 \to \infty$). Following the method proposed by Maillet [29], the thermal quadrupole formalism writes:

$$\begin{bmatrix} \theta_1 \\ \Phi_{12} \end{bmatrix} = [M1][M2] \begin{bmatrix} \theta_2 \\ \frac{\theta_2}{Z} \end{bmatrix} = \begin{bmatrix} 1 & 0 \\ C_1 p & 1 \end{bmatrix} \begin{bmatrix} 1 & R_1 \\ 0 & 1 \end{bmatrix} \begin{bmatrix} \theta_2 \\ \frac{\theta_2}{Z} \end{bmatrix} = \begin{bmatrix} 1 & R_1 \\ C_1 p & 1 + R_1 C_1 p \end{bmatrix} \begin{bmatrix} \theta_2 \\ \frac{\theta_2}{Z} \end{bmatrix} \tag{6}$$

with:
$\theta_1 = \mathcal{L}(T_1(t) - T_1(0))$ being the Laplace transform of the needle temperature variation $[T_1(t) - T_1(0)]$,
$\theta_2 = \mathcal{L}(T_2(t) - T_2(0))$ the Laplace transform of the material temperature variation at the interface needle/material $[T_2(t) - T_2(0)]$,
$\Phi_{12} = \mathcal{L}(\phi_{12})$ the Laplace transform of ϕ_{12},
$M1$ the quadrupolar matrix representing the needle as a pure capacity C_1,
$M2$ the quadrupolar matrix representing the contact resistance at the interface 1-2,
p the Laplace parameter (s^{-1}),
R_1 the thermal contact resistance per unit of length at the interface 1-2 ($\mathrm{m\,K\,W^{-1}}$), and

$$C_1 = \pi(r_e^2 - r_i^2)\rho_1 c_1, \tag{7}$$

$$Z = \frac{K_0(qr_e)}{2\pi\lambda q r_e K_1(qr_e)}, \tag{8}$$

$$q = \sqrt{\frac{p}{a}} \tag{9}$$

where ρ_1 is the density of the needle ($\mathrm{kg\,m^{-3}}$), c_1 the specific heat of the needle ($\mathrm{J\,K^{-1}\,kg^{-1}}$), a the thermal diffusivity of the sample ($\mathrm{m^2\,s^{-1}}$), and λ the thermal conductivity of the sample ($\mathrm{W\,m^{-1}\,K^{-1}}$).

Similarly, we consider a second domain that is bounded by the thermocouple $r_0 = 0 (\approx r_t)$ and the inner needle surface $r_1 = r_i (\approx r_e)$. The quadrupole formalism leads to:

$$\begin{bmatrix} \theta_1 \\ \Phi_{10} \end{bmatrix} = [M3][M4] \begin{bmatrix} \theta_0 \\ 0 \end{bmatrix} = \begin{bmatrix} 1 & R_0 \\ 0 & 1 \end{bmatrix} \begin{bmatrix} 1 & 0 \\ C_0 p & 1 \end{bmatrix} \begin{bmatrix} \theta_0 \\ 0 \end{bmatrix} = \begin{bmatrix} 1 + R_0 C_0 p & R_0 \\ C_0 p & 1 \end{bmatrix} \begin{bmatrix} \theta_0 \\ 0 \end{bmatrix} \tag{10}$$

with:
$\theta_0 = \mathcal{L}(T_0(t) - T_0(0))$ being the Laplace transform of the thermocouple temperature variation $[T_1(t) - T_1(0)]$,
$\Phi_{10} = \mathcal{L}(\phi_{10})$ the Laplace transform of the heat flow rate ϕ_{10},
$M3$ the quadrupolar matrix representing the contact resistance at the interface 0-1,
$M4$ the quadrupolar matrix representing the thermocouple as a pure capacity C_0,
R_0 the thermal contact resistance per unit length between the thermocouple and the needle ($\mathrm{m\,K\,W^{-1}}$), and

$$C_0 = \pi r_t^2 \rho_0 c_0 \tag{11}$$

where ρ_0 is the density of the thermocouple ($\mathrm{kg\,m^{-3}}$) and c_0 the specific heat of the thermocouple ($\mathrm{J\,K^{-1}\,kg^{-1}}$).

From Eq.(6) we deduce:

$$\theta_1 = \left(1 + \frac{R_1}{Z}\right) \theta_2, \tag{12}$$

$$\Phi_{12} = \left(C_1 p + \frac{1 + R_1 C_1 p}{Z}\right) \theta_2 = \left(C_1 p + \frac{1 + R_1 C_1 p}{Z}\right) \frac{\theta_1}{1 + \dfrac{R_1}{Z}}. \tag{13}$$

From Eq.(10) we deduce:

$$\theta_1 = (1 + R_0\, C_0\, p)\, \theta_0, \tag{14}$$

$$\Phi_{10} = C_0\, p\, \theta_0 = \frac{C_0\, p}{1 + R_0\, C_0\, p}\, \theta_1. \tag{15}$$

The Laplace transform of the total heat flow rate ϕ writes:

$$\mathcal{L}(\phi) = \frac{\phi}{p} = \Phi_{12} + \Phi_{10} = \left(\frac{Z C_1 p + 1 + R_1 C_1 p}{Z + R_1} + \frac{C_0 p}{1 + R_0 C_0 p}\right) \theta_1, \tag{16}$$

and by substituting Eq.(14) into Eq.(16) we obtain

$$\theta_0 = \frac{\phi}{p} \frac{Z + R_1}{(Z + R_1)[(C_0 + C_1)p + R_0 C_0 C_1 p^2] + 1 + R_0 C_0 p}. \tag{17}$$

At long time ($p \to 0$), the above equations simplify to:

$$\theta_0 = \frac{\phi}{p}(Z + R_1), \tag{18}$$

$$K_0(qr_e) = -\ln\left(\frac{qr_e}{2}\right) - \gamma, \tag{19}$$

$$K_1(qr_e) = \frac{1}{qr_e}, \tag{20}$$

$$\theta_0(p) = \frac{\phi}{p}\left[-\frac{\ln\left(\frac{qr_e}{2}\right)}{2\pi\lambda} - \frac{\gamma}{2\pi\lambda} + R_1\right] \tag{21}$$

$$= \frac{\phi}{p}\left[-\frac{\ln(p)}{4\pi\lambda} - \frac{\ln\left(\frac{r_e}{2\sqrt{a}}\right)}{2\pi\lambda} - \frac{\gamma}{2\pi\lambda} + R_1\right]. \tag{22}$$

By performing the inverse Laplace transform, we obtain:

$$T_0(t) = \phi\left[\frac{\ln(t)}{4\pi\lambda} + \frac{\gamma}{4\pi\lambda} - \frac{\ln\left(\frac{r_e}{2\sqrt{a}}\right)}{2\pi\lambda} - \frac{\gamma}{2\pi\lambda} + R_1\right], \tag{23}$$

and finally

$$T_0(t) = \frac{\phi}{4\pi\lambda}\ln(t) + \phi\left(\frac{-\gamma}{4\pi\lambda} - \frac{\ln\left(\frac{r_e}{2\sqrt{a}}\right)}{2\pi\lambda} + R_1\right). \tag{24}$$

Equation (24) highlights a logarithm dependence of T_0 with time that becomes the dominant term at long time. This equation is valid only if the regime remains conductive and the medium is infinite. Hence, we can write:

$$T_0(t) = D_1 + D_2 \times \ln(t) \tag{25}$$

with D_1 and D_2 being two constants which depend on the material's thermal conductivity λ. Temperature measurements allow us to identify these two parameters by minimizing $S = \sum_{t_d}^{t_f}(T_{\text{exp}}(t) - T_0(t))^2$ on a time interval $[t_d, t_f]$, where T_{exp} is the experimental temperature measured by the thermocouple and T_0 the temperature obtained from Eq. (25). The thermal conductivity is finally obtained by evaluating the following equation:

$$\lambda = \frac{\phi}{4\pi D_2}. \tag{26}$$

At a given temperature, the experiments are repeated three times and the final value of conductivity is taken as the mean of these experiments. The maximum variation of λ obtained in this way is 0.01 $\mathrm{W\,m^{-1}\,K^{-1}}$.

2.4. Specific heat capacity and latent heat

The specific heat capacity c_p as well as the latent heat of the material are obtained using a Setaram µdSc3 differential calorimeter.

The protocol consists in applying temperature variations to the sample (sample mass about 200 - 300 mg) and in measuring simultaneously the heat transfer over time. In this present study, temperature variations are generated either through ramps of different rates of cooling/heating (1 K $\mathrm{min^{-1}}$, 0.5 K $\mathrm{min^{-1}}$, 0.2 K $\mathrm{min^{-1}}$) or through temperature steps that lead to quasi-steady thermal conditions. In the latter case, steps last long enough in order to recover the steady state, i.e. no more heat flux between the sample and the device. In our experiments, this corresponds to a minimum of 1 hour up to 2 hours per temperature step. Increments between temperature steps are set to 1 K when phase change occurs, i.e. between 283.15 K and 303.15 K, to gain accuracy in evaluating the effective $c_p(T)$. Outside this temperature range, the increment is 2 K. The increment between two successive steps is obtained by applying a temperature ramp of 0.2 K $\mathrm{min^{-1}}$.

Long steps or slow temperature variations have the advantage to avoid or at least to minimize undercooling effects. Reversibility of results are tested performing the entire protocol both increasing and decreasing the temperature. The effective heat capacity is deduced from the heat transferred to the sample after each temperature variation. At the phase transition, the equivalent c_p varies strongly due to the addition of latent heat to sensible heat. The latent heat is therefore estimated by subtracting the sensible heat obtained for the liquid or solid phase from the total heat measured at the phase change.

3. Results

3.1. Density

3.1.1. Liquid phase

Density measurements of PEG 600 are presented in Fig. 5 in the temperature range of [294.15, 373.15] K. Measurements have been performed by cooling the sample in order to avoid any issues related with the formation of bubbles (that occurs when the material is heated over a large temperature range) or with the presence of a mushy phase at the beginning of the analysis, i.e. around 294.15 K. This precaution enables to obtain reproducible density values under our experimental conditions.

Our experimental values are summarized in Fig. 5 together with values currently present in literature [18, 15, 16]. We observe a very good agreement between our results and literature (see also Table 3 where deviations are shown). Our results are found within a maximum difference of 1% from those reported in the above cited studies. Our results can be fitted by a linear model (continuous line in Fig. 5) as follows:

$$\rho(T) = p_1 \times T + p_2 \quad (\mathrm{g\,cm^{-3}}), \tag{27}$$

with $p_1 = -0.00081643$ g cm^{-3} K^{-1}, p_2=1.3652 g cm^{-3} and T the temperature in K. The intervals of the coefficients with 95% confidence bounds are p_1 =[-0.0008182, -0.0008147] and p_2 = [1.365, 1.366].

Furthermore, the thermal expansion coefficient β can be evaluated according to Eq. (1). For instance, at P=1.007 bar, T_{ref} = 298.15 K, we obtain ρ_{ref} = 1.121956 g cm^{-3} and $\beta = 7.28 \times 10^{-4}$ K^{-1} with an estimated combined expanded uncertainty Uc of Uc(β) = 0.02$\times 10^{-4}$ K^{-1} with 0.95 level of confidence (k $\approx$ 2).

3.1.2. Solid phase

The density of PEG 600 in solid phase is obtained using the pycnometer described in section 2.2.2. A material sample of around 150 g is placed in the upper cavity of the pycnometer. The latter is left inside the thermostatic chamber for 24 hours at temperature of 273.75 K. This is done before performing any measurement in order to ensure the complete solidification of the sample. Density measurements are afterward carried out at the same temperature of 273.75 K by keeping the pycnometer with the solid sample inside the thermostatic chamber for the entire duration of the experiment. Two

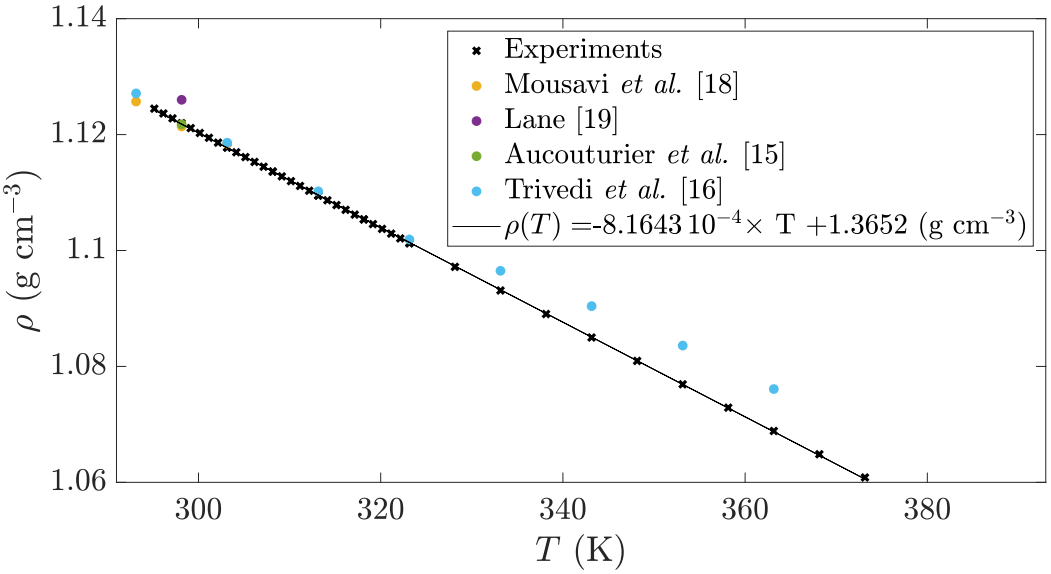

Figure 5: Density ρ of PEG 600 as a function of temperature T at the pressure P=1.007 bar.[a]

[a] Standard uncertainties u are u(P)=0.018 bar, u(T) = 0.01 K and the combined expanded uncertainty Uc is Uc(ρ) =10^{-4} g cm^{-3}

Table 3: Comparison between some of our density measurements (ρ) of PEG 600 with values given in literature (ρ_{ref}) at the pressure P=1.007 bar [a] as function of temperature T

T (K)	ρ ($\times$) (g cm^{-3})	ρ_{ref} ($\circ$) (g cm^{-3})	Reference	Deviation (%)
298.15	1.12196	1.126	[19]	0.36
		1.1214	[18]	0.05
		1.12177	[15]	0.02
303.15	1.11776	1.1184	[18]	0.06
		1.1186	[16]	0.07
313.15	1.10947	1.1102	[16]	0.07
323.15	1.10126	1.1019	[16]	0.06
333.15	1.09310	1.0965	[16]	0.31
343.15	1.08499	1.0904	[16]	0.50
353.15	1.07691	1.0836	[16]	0.62
363.15	1.06886	1.0761	[16]	0.67

[a] Standard uncertainties u are u(P)=0.018 bar, u(T) = 0.01 K and the combined expanded uncertainty Uc is Uc(ρ) =10^{-4} g cm^{-3}

Table 4: Pressure measurements performed for one sample of PEG 600 at 273.75 K.[a]

First set			Second set		
P_i (bar)	P_f (bar)	P_f/P_i	P_i (bar)	P_f (bar)	P_f/P_i
3.317	1.816	54.7 %	3.555	1.943	54.6 %
3.266	1.788	54.7 %	3.365	1.851	54.7 %
3.415	1.869	54.7 %	3.296	1.807	55.0 %
3.548	1.938	54.6 %	3.399	1.861	54.8 %

[a] Standard uncertainties u are u(T)=0.1 K, u(P_i) = 0.002 bar, u(P_f) = 0.002 bar, and the combined expanded uncertainty Uc is Uc(P_f/P_i) = 0.2% with 0.95 level of confidence (k≈2).

sets of pressure measurements are performed in each of which the measurements are repeated 4 times (see Table 4). After the first set of measurement, the sample is removed from the device and melted. The protocol is then performed again for the second set.

For the range of PEG volume involved in our experiments, the error of measurements is found smaller than 5%. This value is obtained using a stainless steel sample with a known volume of 3.92×10^{-5} m^3. The volume measured with the pycnometer led to $V_{sample} = 3.82 \times 10^{-5}$ m^3, i.e. within 2.6 % difference with the real value.

The density of PEG 600 in solid phase is evaluated to $\rho = 1510 \pm 23$ kg m^{-3} at 273.75 K, value that is quite different from the one obtained for the liquid phase. This is not surprising as it is correlated to the large variation in volume occurring during solidification.

3.2. Thermal conductivity

3.2.1. Liquid phase - Steady hot tube method

As above mentioned in section 2.3.1, the steady hot tube method is relevant only in the liquid phase as it requires good thermal contacts between the sample and the tubes surfaces. Since the device is filled with PEG 600 in liquid phase, the largest decrease in volume that leads to thermal resistances at interfaces is observed at the liquid-to-solid transition. At temperature below 293.15 K results are indeed no longer reproducible. For higher temperatures, however, surface contact resistances can be assumed to be negligible. Measurements are performed at steady state. Results obtained with this device are presented in Fig. 6 ('+' symbols) as a function of the mean temperature between the two thermocouples, i.e. $\bar{T} = T = (T_1 + T_2)/2$. Additional val-

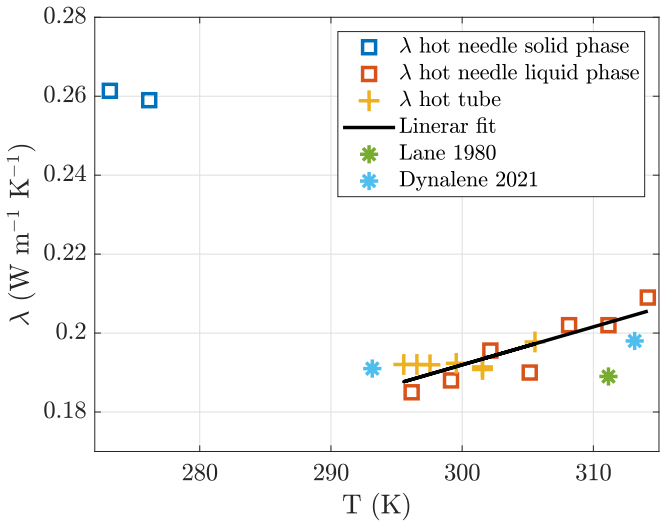

Figure 6: Thermal conductivity results for liquid phase and solid phases at the pressure P=1.007 bar[a]. The temperature T refers (i) to the mean temperature between thermocouples $T = \bar{T} = (T_1+T_2)/2$ in the case of the hot tube method and (ii) to the temperature in the thermostatic enclosure in the case of the hot needle method.

[a] Standard uncertainties u are u(P)= 0.018 bar, u(T) = 0.1 K, u(I) = 0.1 A, and the combined expanded uncertainty Uc is Uc(λ) = 0.01 W m^{-1} K^{-1} with 0.95 level of confidence (k≈2) for hot tube method from eq. (3) and eq. (26)

ues of thermal conductivity given by Lane [19] and values from a data sheet provided by Dynalene [30] are also displayed in Fig. 6 for comparison. In our experiments the temperature variation $\Delta T = T_2 - T_1$ does not exceed 3 K through the annular region of the device, i.e. between r_1 and r_2. In the range of the tested temperatures, we observe a slight temperature dependence of λ. These measurements are complemented by those obtained by using the hot needle method.

3.2.2. Solid and liquid phases - Hot needle method

The measurements are carried out with the needle probe described previously in Section 2.3.2. The estimation of the thermal conductivity λ is obtained assuming: (i) conductive regime in the vicinity of the needle, (ii) an infinite medium and (iii) $T_0(t) \propto \ln(t)$ at long time. The time interval $[t_i, t_f]$, in which the latter condition is satisfied, is determined empirically when the difference between experiments and the model is close to zero (see the discussion below about residuals).

Thermal conductivity values in the solid phase are obtained placing the

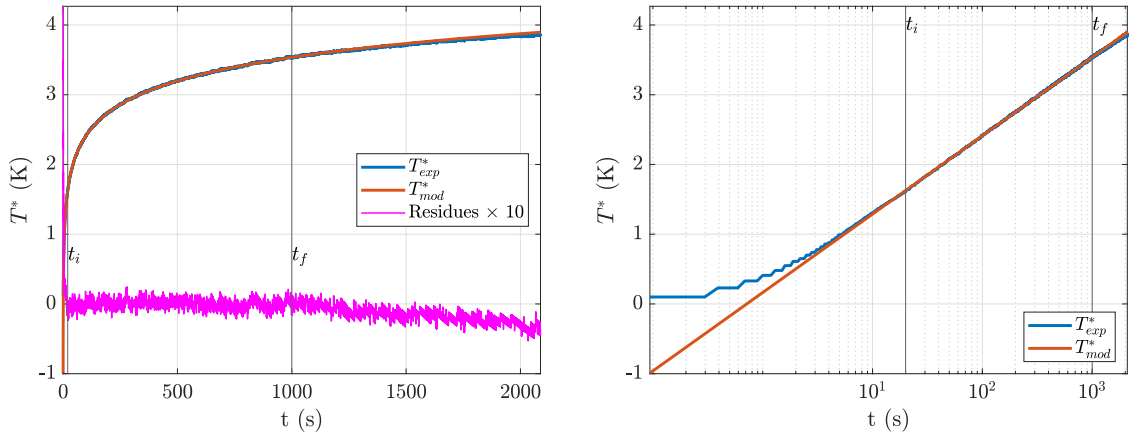

(a) Linear scale

(b) Semi-log scale

Figure 7: Time evolution of experimental ($T^*_{\rm exp}$, in blue) and simulated ($T^*_{\rm mod}$, in red) temperature difference T^* between the hot needle and the thermostatic enclosure set at 276.15 K and P=1.007 bar. The red curve is obtained with the simplified model from Eq. (25). Magenta curve in (a) displays the residues S between $T_{\rm exp}$ and $T_{\rm mod}$ multiplied by 10 times.

device in the temperature controlled binder. An example of temperature measurement ($T^* = T_0(t) - T_0(0)$) is plotted in Fig. 7 as a function of time. In the same figure we also display temperature values estimated by the model given by Eq. (25). Residuals multiplied by 10 times are also plotted in order to highlight the differences between measurements and the model. For each set of experiments, we determine the time interval $[t_i, t_f]$ along which residuals are perfectly flat and centered on zero, i.e. the time interval in which our model is consistent. This interval is bounded by vertical lines in Figs. 7 and 8. In the case presented in Fig. 7, the estimation time interval is [20, 1000] s. The divergence of the residuals after 1000 s indicates the limit of validity of the infinite medium assumption. Following Eq. (25), we evaluate D_2 within the estimation interval as the slope of the temperature variation with time in semi-log scale (Fig. 7b).

The model also applies to the liquid phase only if convection does not occur. For this reason, we have also performed some measurements above 293.15 K. We show them in Fig. 8, where experimental and simulated temperature variations are displayed as a function of time. The same conditions described above are assumed and residuals are again plotted multiplied by 10 times. Figure 8 corresponds to two different temperatures imposed in the

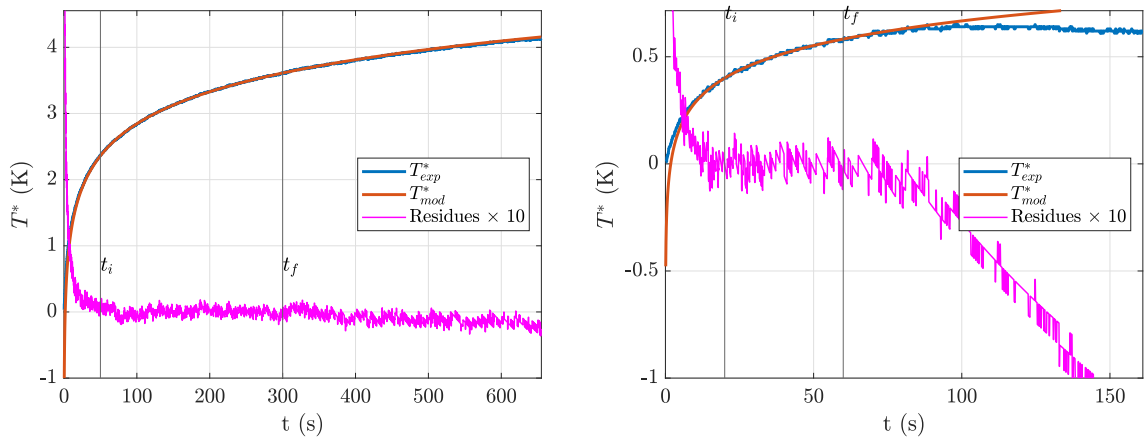

(a) 299.15 K

(b) 314.15 K

Figure 8: Time evolution of experimental (T^*_{exp}, in blue) and simulated (T^*_{mod}, in red) temperature difference T^* between the hot needle and the thermostatic enclosure set at P=1.007 bar and 299.15 K (a) and 314.15 K (b). The red curve is obtained with the simplified model from Eq. (25). Magenta curves display the residues between T^*_{exp} and T^*_{mod} multiplied by 10 times.

chamber, i.e. 299.15 K and 314.15 K. The estimation interval was adjusted to [50, 300] s for the measurement at 299.15 K and to [20, 60] s for the measurement at 314.15 K. The residuals are found flat and centered on zero over these intervals. In the case of 314.15 K, the divergence of the residuals after 60 s is explained by the occurrence of convection around the needle. The higher the temperature is, the earlier this phenomenon appears. For instance, convection is not observed before 300 s for the case at 299.15 K.

Figure 6 summarizes all the thermal conductivity measurements as a function of temperature carried out for PEG 600. In liquid phase, values obtained via the needle method (squares) are consistent with the ones obtained using the hot tube method. The thermal conductivity in liquid phase shows a slight increase with increasing temperature following a linear variation: $\lambda(T) = 9.61 \times 10^{-4}\,T - 9.66 \times 10^{-2}$, with λ in $\mathrm{W\,m^{-1}\,K^{-1}}$ and temperature T in K. The intervals of the coefficients with 95% confidence bounds are p_1 = [0.0006076, 0.001316] and p_2 = [-0.2037, 0.01055].

Our results are also very close to those provided by Dynalene (see the data sheet in [30]), i.e. $\lambda = 0.191$ $\mathrm{W\,m^{-1}\,K^{-1}}$ at 293.15 K and $\lambda = 0.198$ $\mathrm{W\,m^{-1}\,K^{-1}}$ at 313.15 K. A good agreement is also found with values published by Lane [19], who obtained $\lambda = 0.189$ $\mathrm{W\,m^{-1}\,K^{-1}}$ at 311.00 K and

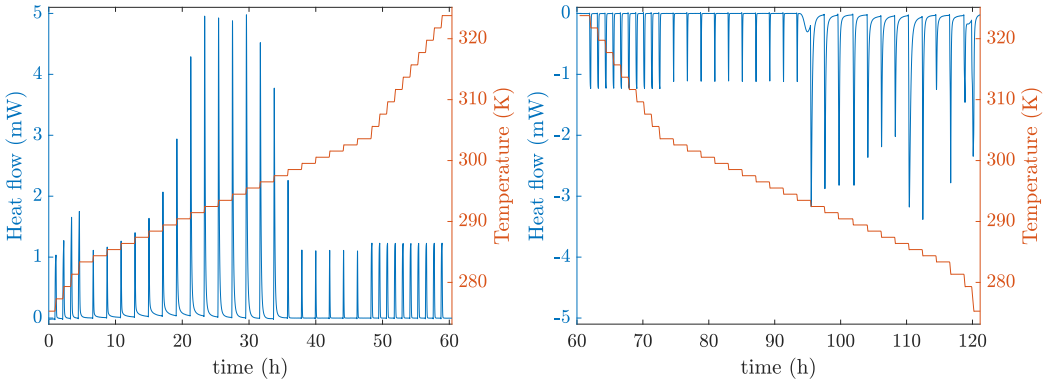

(a) Melting (endothermic process)

(b) Solidification (exothermic process)

Figure 9: Heat flow rate measured from DSC (in blue) and imposed temperature steps (in red) as a function of time. (a) Melting of PEG 600 for increasing temperature steps (endothermic process). (b) Solidification of PEG 600 for decreasing temperature steps (exothermic process)[a] at the pressure P=1.007 bar.
[a] Standard uncertainties u are u(P)=0.018 bar, u(Heat flow) = 0.01 mW and u(T)=0.01K.

$\lambda = 0.187\ \mathrm{W\,m^{-1}\,K^{-1}}$ at 340.15 K.

In solid phase, the value of conductivity measured at 273.15 K and 276.15 K does not vary much, leading for this temperature interval to $\lambda_s \approx 0.260\ \mathrm{W\,m^{-1}\,K^{-1}}$. This value is close to the one proposed by Kou et al [14] for PEG 1000, i.e. $0.29 \pm 0.05\ \mathrm{W\,m^{-1}\,K^{-1}}$. In our experiments, for an enclosure temperature of 279.15 K, the temperature near the needle is around 283.00 K and the material starts to melt. For this reason, it is difficult to obtain λ of PEG 600 in solid phase above 276.15 K. The gap between 276.15 K and 293.15 K in terms of thermal conductivity (Fig. 6) is explained by the occurrence of the phase transition.

To summarize, our measurements provide values of thermal conductivity in each liquid and solid phase. An effective value of λ in solid phase can be measured in the temperature range [276.15, 293.15] K. However we think that a careful investigation of the material structure at the phase transition would be more relevant. This aspect is beyond the scope of this present article but it will be investigated in the near future.

3.3. Specific heat capacity and latent heat

Raw data obtained by differential scanning calorimetry are presented in Fig. 9 for the case of imposed temperature steps (in red). The figure displays the amount of heat flux (in blue) transferred between the PCM sample and the calorimeter. Each increment of temperature leads to a peak in terms of heat exchanged. The latter goes back to zero as soon as the thermal equilibrium is reached. Given this experimental protocol, the effective heat capacity c_p is deduced by integrating the heat flux over the duration of a step (including the increment) and dividing it by the mass of the sample m and the temperature increment.

On the other hand, if the protocol involves temperature ramps, i.e. continuous temperature variations with time, we directly determine the effective c_p from the measured heat flux ϕ according to

$$\phi = m c_p \frac{dT}{dt}, \tag{28}$$

where the temperature variations rate $\dfrac{dT}{dt}$ is constant and imposed by the ramp. We deduce then:

$$c_p = \frac{\phi}{m} \left(\frac{dT}{dt} \right)^{-1}. \tag{29}$$

The resulting values of effective c_p are shown in Fig. 10 as a function of temperature. Similar trends are observed between the two protocols. When the material is liquid, i.e. for large temperature values (above 298.15 K) and at pressure P=1020 $\pm$ 0.018 bar, we obtain a quasi constant heat capacity $c_p = 2.13 \pm 0.05$ kJ kg^{-1} K^{-1} (corresponding to 1278 ± 30 J K^{-1} mol^{-1}). This value is recovered in the liquid phase for both cooling and heating experiments.

Similarly, when the material is solid, i.e. for low temperature values (below 283 K) and P=1020 $\pm$ 0.018 bar, we obtain $c_p = 2.74 \pm 0.05$ kJ kg^{-1} K^{-1} (corresponding to 1644 ± 30 J K^{-1} mol^{-1}).

In the temperature range where the phase transition occurs (i.e. solidification in Fig. 10a and melting in Fig. 10b), variations in the evaluated c_p are due to the competition between the kinetics of the phase change process and the rate of temperature variations. This competition leads to a temperature hysteresis during solidification that corresponds to undercooling effects. This latter phenomena decreases for slow temperature variations. In the case

of imposed temperature steps, the melting of PEG 600 is observed between 283.15 K and 295.15 K, while its solidification occurs between 293.15 K and 283.15 K. Further differences between melting and freezing processes can be highlighted. Indeed, two distinct local maxima are observed during solidification as the temperature decreases (Fig. 10a). These extrema are always obtained for similar temperature values when the adopted cooling protocol lasts long enough. Here, extrema correspond to exothermal transformations correlated to structural modifications that occur during the crystallization [20, 21]. Whatever the protocol used, the integration of only the part due to the phase transition in the effective heat capacity leads to a latent heat of 130 ± 0.55 kJ kg^{-1}. Reciprocally, at least one extremum value in terms of c_p is also obtained for the melting process (Fig. 10b). When the heating process is long enough (0.2 K min^{-1}), two local peaks are observed but their amplitudes are smaller than in the case of the solidification process. These multiple peaks are observed also in other studies that attribute them to microstructural variations, i.e. crystals with different thickness due to variations in folds number in the polymer chain [31] or due to the evolution of the lamellar microstructure during the phase change [32]. The latent heat is evaluated as before and values obtained from different protocols converge to 127 ± 0.55 kJ kg^{-1}. The latter is close to what obtained for the solidification process. Furthermore, our values are in very good agreement with the one proposed by Lane [19], i.e. 127.2 kJ kg^{-1}. According to Pielichowski & Flejtuch [33], the latent heat of melting of 100% crystalline polymer is 196.8 kJ kg^{-1}. Compared with this latter value, PEG 600 should correspond to a degree of crystallinity of 64.5%. Indeed, low molecular weight polymers are known to have higher segmental mobility, thus reducing the formation of the crystalline phase (geometric alignment), as observed for PEG at different molecular weight [14, 33].

4. Conclusion

In this study we report the thermal properties of polyethylene glycol 600 (PEG 600). The density in liquid phase has been measured in the temperature range [298.15, 373.15] K. Given the small temperature increments used, we have been able to provide a fit for the temperature-dependent density of liquid PEG 600. The latter allows to determine the coefficient of thermal volume expansion with a good accuracy. The density of PEG 600 in solid phase has been measured by using a pycnometer and it results in $\rho = 1510$

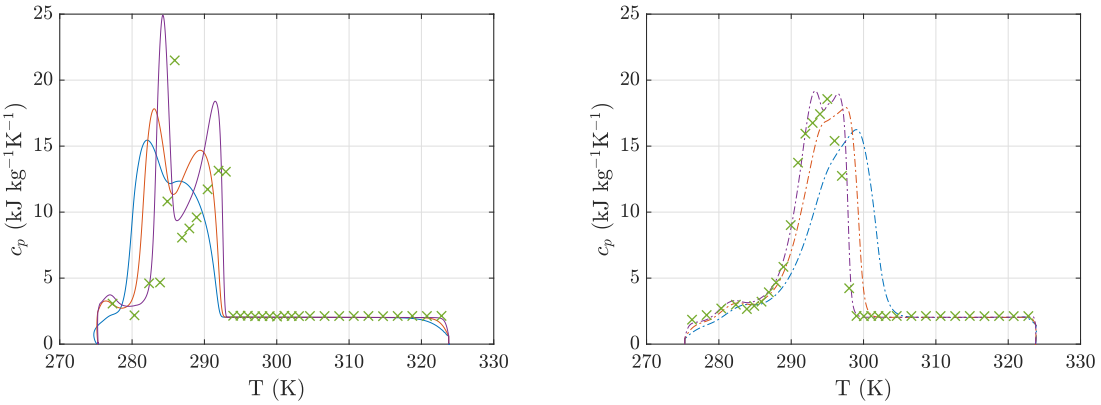

(a) Solidification (exothermal transformation)

(b) Melting (endothermal transformation)

Figure 10: Effective $c_p(T)$ evaluated during (a) the solidification process and (b) the melting process, for temperature variations of 1 K min^{-1} (blue lines), 0.5 K min^{-1} (red lines), 0.2 K min^{-1} (purple lines) and temperature steps (green crosses) at P=1.007 bar [a] [a] Standard uncertainties u are u(P)=0.018 bar, u(Heat flow)=0.01 mW, u(T) = 0.01 K, u(m)= 0.01 mg and the combined expanded uncertainty Uc is Uc(c_p) = 0.05 kJ kg^{-1} K^{-1} with 0.95 level of confidence (k≈ 2)

kg m^{-3} at 273.75 K. The variation of density between the two phases highlights a quite large volume shrinkage of the material during solidification. This can have a drastic consequence on thermal contacts at interfaces and hence a strong impact in the usability of this PCM in thermal energy storage systems.

The thermal conductivity λ has been investigated with two different methods. Results for the liquid phase show a slight linear increase of λ with increasing temperature, while for the solid phase we find $\lambda_s \approx 0.260$ W m^{-1} K^{-1} within the investigated temperature range.

Effective heat capacity and heat transfer have been described and quantified by DSC measurements. Far from the phase transition, we obtain a constant specific heat capacity for both solid and liquid phase. The phase transition occurs between 283.15 K and 298.15 K, depending whether the sample is cooled or heated. Undercooling effects are responsible for the hysteresis in phase change temperature, however they decrease when the cooling rate is decreased. For the different protocols tested in DSC, we obtain a similar value for the latent heat, i.e. 130 kJ kg^{-1}. Furthermore, during the solidification process we observe several exothermic peaks that highlight reorganizations of aggregates and/or crystals in the internal structure of PEG

600. This latter aspect is beyond the scope of this study. However, since explanations on PEG crystallization are still controversial in literature, a proper investigation at small scales of this process will be a fundamental part of our future work.

Appendix A. Estimation of the error due to steady-state contact resistances

During solidification, the density of the sample increases and $\rho_l < \rho_s$, with ρ_l being the density of the liquid phase and ρ_s the one of the solid phase. This results in a decrease in volume with temperature. In the hot tube device used to measure the thermal conductivity, this leads to an air/vacuum layer of thickness ϵ between the sample and the inner heating tube of radius r_1 (Fig. 2).

One can write:

$$\rho_l \pi (r_2^2 - r_1^2) = \rho_s \pi [r_2^2 - (r_1 + \epsilon)^2], \tag{A.1}$$

leading to

$$\epsilon = \left[r_2^2 - \frac{\rho_l}{\rho_s}(r_2^2 - r_1^2) \right]^{0.5} - r_1.$$

The thermal resistance between the two tubes is:

$$R = \frac{1}{2\pi\lambda} \ln\left(\frac{r_2}{r_2 - r_1 - \epsilon}\right) + \frac{1}{2\pi\lambda_{air}} \ln\left(\frac{r_1 + \epsilon}{r_1}\right) = \frac{1}{2\pi\lambda_m} \ln\left(\frac{r_2}{r_1}\right). \tag{A.2}$$

In this way, λ_m is the measured value of the thermal conductivity while λ is the real thermal conductivity of the solid sample. We deduce:

$$\lambda_m = \ln\left(\frac{r_2}{r_1}\right) \left[\frac{1}{\lambda} \ln\left(\frac{r_2}{r_2 - r_1 - \epsilon}\right) + \frac{1}{\lambda_{air}} \ln\left(\frac{r_1 + \epsilon}{r_1}\right) \right]^{-1}. \tag{A.3}$$

The radii values are $r_1 = 2.75$ mm; $r_2 = 6$ mm. With an estimated value for the thermal conductivity in solid phase of $\lambda = 0.26\ \mathrm{W\,m^{-1}\,K^{-1}}$, we can calculate the value λ_m that we would have measured with the hot tube method. For ρ_l/ρ_s =0.75, the calculation leads to $\lambda_m = 0.19\ \mathrm{W\,m^{-1}\,K^{-1}}$, i.e. around 30% less than the actual value. For this reason, the steady-state hot tube device used in this study to measure λ of liquid PEG 600 is unsuitable to retrieve λ of the solid phase. For measurements of thermal conductivity of solid PCMs is therefore preferable to use a transient measurement device where contact resistances have no influence on estimating the conductivity.

Acknowledgments

Financial supports have been brought to this work by the operation "STOCK'NRJ" co-financed by the European Union within the framework of the Program FEDER-FSE Lorraine and Massif des Vosges 2014-2020.

References

[1] M. Kobayashi, T. Koide, S.-H. Hyon, Tribological characteristics of polyethylene glycol (PEG) as a lubricant for wear resistance of ultra-high-molecular-weight polyethylene (UHMWPE) in artificial knee join, Journal of the Mechanical Behavior of Biomedical Materials 38 (2014) 33–38.

[2] K. Bjugstad, D. Redmond Jr, K. Lampe, D. Kern, J. Sladek Jr, M. Mahoney, Biocompatibility of PEG-based hydrogels in primate brain, Cell Transplantation 17 (4) (2008) 409–415.

[3] A. K. Jain, A. K. Goyal, N. Mishra, B. Vaidya, S. Mangal, S. P. Vyas, PEG–PLA–PEG block copolymeric nanoparticles for oral immunization against hepatitis B, International Journal of Pharmaceutics 387 (1-2) (2010) 253–262.

[4] S. M. Baygi, S. Sadrameli, Thermal management of photovoltaic solar cells using polyethylene glycol 1000 (PEG1000) as a phase change material, Thermal Science and Engineering Progress 5 (2018) 405–411.

[5] F. Hamad, E. Egelle, K. Cummings, P. Russell, Investigation of the melting process of polyethylene glycol 1500 (PEG 1500) in a rectagular enclosure, International Journal of Heat and Mass Transfer 114 (2017) 1234–1247.

[6] J. Wang, M. Yang, Y. Lu, Z. Jin, L. Tan, H. Gao, S. Fan, W. Dong, G. Wang, Surface functionalization engineering driven crystallization behavior of polyethylene glycol confined in mesoporous silica for shape-stabilized phase change materials, Nano Energy 19 (2016) 78–87.

[7] J. Yang, E. Zhang, X. Li, Y. Zhang, J. Qu, Z.-Z. Yu, Cellulose/graphene aerogel supported phase change composites with high thermal conductivity and good shape stability for thermal energy storage, Carbon 98 (2016) 50–57.

[8] J. Jin, F. Lin, R. Liu, T. Xiao, J. Zheng, G. Qian, H. Liu, P. Wen, Preparation and thermal properties of mineral-supported polyethylene glycol as form-stable composite phase change materials (CPCMs) used in asphalt pavements, Scientific Reports 7 (1) (2017) 1–10.

[9] Y. Zhou, X. Liu, D. Sheng, C. Lin, F. Ji, L. Dong, S. Xu, H. Wu, Y. Yang, Graphene oxide/polyurethane-based solid–solid phase change materials with enhanced mechanical properties, Thermochimica Acta 658 (2017) 38–46.

[10] A. Sharma, V. V. Tyagi, C. Chen, D. Buddhi, Review on thermal energy storage with phase change materials and applications, Renewable and Sustainable Energy Reviews 13 (2) (2009) 318–345.

[11] B. Zalba, J. M. Marın, L. F. Cabeza, H. Mehling, Review on thermal energy storage with phase change: materials, heat transfer analysis and applications, Applied Thermal Engineering 23 (3) (2003) 251–283.

[12] M. Firoozzadeh, A. H. Shiravi, M. Shafiee, Experimental and analytical study on enhancing efficiency of the photovoltaic panels using Polyethylene-Glycol 600 (PEG 600) as a phase change material, Iranian Journal of Energy and Environment 10 (2019) 23–32. doi:10.5829/ijee.2019.10.01.04.

[13] R. Velraj, R. Seeniraj, B. Hafner, C. Faber, K. Schwarzer, Heat transfer enhancement in a latent heat storage system, Solar Energy 65 (3) (1999) 171–180.

[14] Y. Kou, S. Wang, J. Luo, K. Sun, J. Zhang, Z. Tan, Q. Shi, Thermal analysis and heat capacity study of polyethylene glycol (PEG) phase change materials for thermal energy storage applications, The Journal of Chemical Thermodynamics 128 (2019) 259–274.

[15] C. Aucouturier, G. Roux-Desgranges, A. Roux, Excess molar volumes and excess molar heat capacities of (polyethylene glycols+ water) at temperatures between T=278 K and T=328 K, The Journal of Chemical Thermodynamics 31 (2) (1999) 289–300.

[16] S. Trivedi, C. Bhanot, S. Pandey, Densities of poly(ethylene glycol)+ water over the temperature range (283.15 to 363.15) K, The Journal of Chemical Thermodynamics 42 (11) (2010) 1367–1371.

[17] A. Singh, R. Walvekar, M. Khalid, W. Y. Wong, T. Gupta, Thermophysical properties of glycerol and polyethylene glycol (PEG 600) based DES, Journal of Molecular Liquids 252 (2018) 439–444.

[18] Z. Mousavi, M. Pirdashti, A. A. Rostami, E.-N. Dragoi, Thermophysical properties analysis of poly (ethylene glycol) 600+ methanol, ethanol, 1-propanol, and 2-propanol binary liquid mixtures, International Journal of Thermophysics 41 (2) (2020) 1–26.

[19] G. A. Lane, Low temperature heat storage with phase change materials, International Journal of Ambient Energy 1 (3) (1980) 155–168.

[20] L. Yang, T. Smith, Melting and solidification behavior of blends of high density polyethylene with poly (butylene terephthalate), Polymer Engineering & Science 33 (21) (1993) 1426–1430.

[21] A. Azri, P. Giamarchi, Y. Grohens, R. Olier, M. Privat, Polyethylene glycol aggregates in water formed through hydrophobic helical structures, Journal of Colloid and Interface Science 379 (1) (2012) 14–19.

[22] B. Bogdanov, A. Vidts, E. Schacht, H. Berghmans, Isothermal crystallization of poly (ε-caprolactone- ethylene glycol) block copolymers, Macromolecules 32 (3) (1999) 726–731.

[23] K. Pielichowski, K. Flejtuch, Differential scanning calorimetry studies on poly (ethylene glycol) with different molecular weights for thermal energy storage materials, Polymers for Advanced Technologies 13 (10-12) (2002) 690–696.

[24] D. D. Gray, A. Giorgini, The validity of the Boussinesq approximation for liquids and gases, International Journal of Heat and Mass Transfer 19 (5) (1976) 545–551.

[25] Y. Jannot, A. Degiovanni, Thermal properties measurement of materials, John Wiley & Sons, 2018.

[26] N. R. Sgreva, J. Noel, C. Metivier, P. Marchal, H. Chaynes, M. Isaiev, Y. Jannot, Thermo-physical characterization of hexadecane during the solid/liquid phase change, Thermochimica Acta (2022) 179 – 180.

[27] J. Huetz, J.-P. Petit, Notions de transfert thermique par convection, Techniques de l'Ingénieur (A1504A) (Aug. 1990).

[28] A. I. Brown, S. M. Marco, Introduction to heat transfer, 3rd Edition, Mc Graw-Hill Book Company, New York, 1958.

[29] D. Maillet, S. Andre, J. C. Batsale, A. Degiovanni, C. Moyne, Thermal quadrupoles: solving the heat equation through integral transforms, Wiley-Blackwell, 2000.

[30] Dynalene Inc., PEG Series: Techincal data sheet, https://www.dynalene.com/product-category/heat-transfer-fluids/polyethylene-glycol-heat-transfer-fluids/.

[31] B. Wunderlich, Macromolecular physics: Crystal nucleation, Growth, Annealing 2 (1976).

[32] M. S. Lisowski, Q. Liu, J. Cho, J. Runt, F. Yeh, B. S. Hsiao, Crystallization behavior of poly (ethylene oxide) and its blends using time-resolved wide-and small-angle X-ray scattering, Macromolecules 33 (13) (2000) 4842–4849.

[33] K. Pielichowski, K. Flejtuch, Differential scanning calorimetry studies on poly(ethylene glycol) with different molecular weights for thermal energy storage materials 13 (10) 690–696, _eprint: https://onlinelibrary.wiley.com/doi/pdf/10.1002/pat.276. doi:10.1002/pat.276.
URL http://onlinelibrary.wiley.com/doi/abs/10.1002/pat.276